

when the gaps are centered or each ridge is a symmetrical double ridge. Some additional information is given in Fig. 3, where, for a fixed ridge width ( $s/a$ ) and two values of ridge spacing ( $t/a$ ), the variations of the normalized cutoff wavelength ( $\lambda_{c-}/a$ ) and the bandwidth  $B$  with gap width ( $d/b$ ) are shown for a regular structure with two symmetrical double ridges and an inverted structure with two single ridges.

### B. Eigenvector and Gap Impedance

To solve the eigenvector  $C_N^{(j,k)}$  in (10) was expressed in terms of  $C_l^{(j,k)}$  and inverted submatrices after further manipulations. However, these expressions were not useful for numerical computation, as the diagonal elements of diagonal matrices  $H_2$  and  $H_7$ , are all zero after the first few leading elements, which cause failure in numerical inversion. The actual computation of the eigenvector components was carried out by a Gauss-Siedel iteration of (10) with  $C_l^{(j,k)}$  made arbitrary successively (usually unity prior to normalization of the eigenvector). The matrix  $[H]$  being diagonally dominant, the convergence was excellent.

The variation of  $Z_{g(\infty)}$  at the gap center ( $\rho = 0.5$ ) with  $(d/b)$  for the dominant TE mode in an inverted structure with two single ridges is shown in Fig. 3. For a given set of parameters ( $t/a$ ), ( $s/a$ ), and  $(d/b)$ , this impedance is found to be almost independent of gap height ( $h/b$ ), that is, almost identical for the regular and inverted structures. For given  $(s/a)$  and  $(d/b)$ , however, it varies considerably with ridge spacing ( $t/a$ ) in either case. The impedance curves in Fig. 3 also closely depict those for the regular structure with two symmetrical double ridges of identical parameters, with the difference of impedance in the two cases being less than 0.5 percent.

### V. RIDGED WAVEGUIDE VARACTOR-TUNED GUNN OSCILLATOR

In this section, some preliminary experimental results obtained with two empirically-designed  $XN$ -band varactor-tuned Gunn oscillators in fixed-length ridged-waveguide resonators are presented. The device mounts were not optimized and the choice of ridge parameters was guided purely by mechanical considerations. Fig. 4(a) shows the schematic diagrams of the device mount in an inverted ridged WR-137 waveguide resonator (referred to as oscillator A). For the oscillator with a resonator in regular configuration (referred to as oscillator B), all the dimensions except the ridge spacing were identical. The performance of these two oscillators is shown in Fig. 4(b), where the measured shift in oscillation frequency and the output power are plotted as functions of varactor bias.

### VI. CONCLUSIONS

The Ritz-Galerkin technique has been applied to determine the eigenvalues of a rectangular waveguide with two double ridges located arbitrarily. When two identical, asymmetric double ridges are placed symmetrically, considerable improvement in bandwidth occurs if one ridge is inverted with respect to the other. The best result is obtained when two single ridges are closely spaced in an inverted configuration. The eigenvector has been obtained by iteration of the matrix equations and has been used in determining the gap impedance. Finally, the same preliminary results obtained with two  $XN$ -band varactor-tuned Gunn oscillators in regular and inverted ridged resonators have been presented. Though there is scope for optimization of the device mounts, the results are certainly promising for such applications of the ridged waveguides.

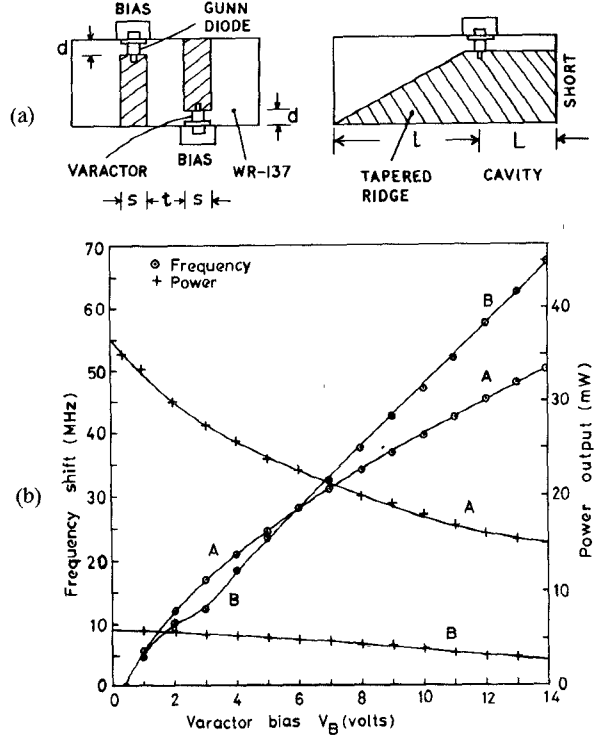


Fig. 4. (a) Varactor-tuned Gunn oscillator in inverted waveguide resonator (waveguide: WR-137).  $s = 0.25$  in.,  $d = 0.1$  in.,  $L = 1.75$  in.,  $L = 0.875$  in.,  $t = 0.157$  in. (OSC.A);  $0.295$  in. (OSC.B). (b) Variation of frequency shift and power output with varactor bias ( $V_B$ ). Frequency of oscillation at  $V_B = 0.4$  V: 7.495 GHz (OSC.A); 7.20 GHz (OSC.B). Varactor diode: AEI DC 4201B, Gunn diode: MA 49151 (OSC.A); MA 49156 (OSC.B).

### ACKNOWLEDGMENT

The authors are thankful to Professor B. R. Nag for his encouragement during the work, and to the Computer Centre, Calcutta University, for the use of their IBM 1130 computer. The helpful suggestions from the reviewers are very much appreciated.

### REFERENCES

- [1] J. P. Montgomery, "On the complete eigenvalue solution of ridged waveguide," *IEEE Trans. Microwave Theory Tech.*, vol. MTT-19, pp. 547-555, June 1971.
- [2] D. Dasgupta and P. K. Saha, "Eigenvalue spectrum of rectangular waveguide with two symmetrically placed double ridges," *IEEE Trans. Microwave Theory Tech.*, vol. MTT-29, pp. 47-51, Jan. 1981.
- [3] E. V. Jull, W. J. Bleackley, and M. M. Steen, "The design of waveguide with symmetrically placed double ridges," *IEEE Trans. Microwave Theory Tech.*, vol. MTT-17, pp. 397-399, July 1969.

### Mutual Impedance Computation Between Microstrip Antennas

E. H. NEWMAN, MEMBER, IEEE, J. H. RICHMOND, FELLOW, IEEE, AND B. W. KWAN

**Abstract**—A moment-method solution for the mutual coupling between rectangular microstrip antennas is presented. The grounded dielectric slab is accounted for exactly in the analysis.

Manuscript received May 11, 1982; revised June 23, 1983. This work was supported in part by the Department of the Army under Grant DAAG29-81-K-0020 and by the Joint Services Electronics Program under Contract N00014-78-C-0049 with The Ohio State University Research Foundation.

The authors are with the Ohio State University Electro Science Laboratory, Department of Electrical Engineering, Columbus, Ohio 43212.

## I. INTRODUCTION

A microstrip antenna is a thin metallic patch printed on a grounded dielectric slab. The fact that they are lightweight, flush mountable, and inexpensive to fabricate has resulted in considerable interest and application of these antennas. Recently, a special issue of the IEEE TRANSACTIONS ON ANTENNAS AND PROPAGATION [1] was devoted to microstrip antennas. Much of the theoretical or computational work on microstrip antennas has dealt with the isolated element. The analysis of mutual coupling between microstrips is important in the design of antenna arrays, especially if tight pattern control or low sidelobes is required. Alexopoulos and Rana [2] have employed the method of moments (MM) to compute the mutual impedance between extremely narrow printed circuit dipoles. Here, we employ the method of moments to compute the mutual impedance between microstrip antennas. This work differs from that previously done by one of the authors [3], in that here the grounded dielectric slab is accounted for in an exact manner.

## II. MOMENT-METHOD SOLUTION

In this section, we will outline the moment-method solution for coupled microstrip antennas. Fig. 1 shows two rectangular microstrip antennas on a grounded dielectric slab. Patch 1 is excited by a constant 1-A current,  $J_i = \hat{z}$  A, which is a reasonable approximation to a coaxial or edge feed [3]. The surface current,  $J_s$ , on the microstrip patches is a solution of the symbolically written integral equation

$$E_s + E_i = 0 \quad (1)$$

for the tangential fields on the microstrip patches. Here,  $J_s$  is the vector sum of the current on the top and bottom surfaces of the patches, and  $E_s$  and  $E_i$  are the electric fields radiated by  $J_s$  and  $J_i$ , respectively, in the presence of the grounded dielectric slab. Using reciprocity and the zero reaction concept, (1) can be written as the reaction integral equation [4]

$$-\int_S \int J_s \cdot E_T ds = \int_L J_i \cdot E_T dl \quad (2)$$

where the surface integral is over the surface of the microstrip patches (where  $J_s$  exists) and the line integral is over the length of  $J_i$ .  $E_T$  is the electric field, in the presence of the grounded dielectric slab, of an arbitrary test surface current  $J_T$  located on  $S$ .

Equation (2) will be solved for  $J_s$  by the numerical technique known as the MM [5]. The MM can transform a linear integral equation, which may have no known exact solution, into a system of simultaneous linear algebraic equations which can be easily solved via matrix algebra. Under the proper circumstances, the solution of the simultaneous linear equations provides an excellent approximation to the integral equation [5]. The MM solution closely parallels the authors previously published solution for conducting plates in free space [6]. However, for completeness, it will be briefly reviewed here.

Although (2) must apply for an arbitrary test current  $J_T$ , we will enforce (2) for only a finite sequence of test currents, usually called test modes. If we place  $I$  test modes on the first microstrip patch and  $J$  on the second, then we will have a total of  $N = I + J$  test modes denoted  $J_m$  ( $m = 1, 2, \dots, N$ ). These test modes can be any  $N$  linearly independent current shapes on the patches. Enforcing (2) for each  $J_m$  yields the system of simultaneous integral equations

$$-\int_S \int J_s \cdot E_m ds = \int_L J_i \cdot E_m dl \quad m = 1, 2, \dots, N \quad (3)$$

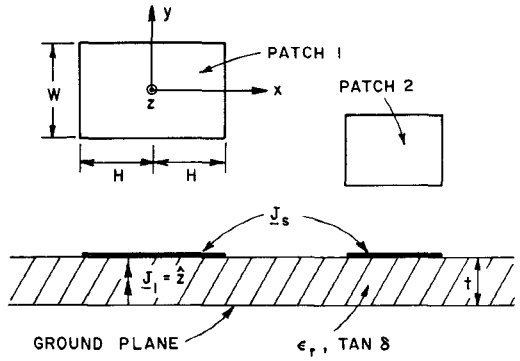


Fig. 1. Two coupled microstrip antennas on a grounded dielectric slab.

where  $E_m$  is the field of  $J_m$  in the presence of the grounded dielectric slab.

The next step in the MM solution is to expand the current  $J_s$ . If we use  $I$  expansion modes on the first patch and  $J$  modes on the second, then

$$J_s = \sum_{n=1}^N I_n J_n \quad (4)$$

where the  $J_n$  ( $n = 1, 2, \dots, N$ ) are a sequence of known current functions, termed expansion modes, and the  $I_n$  ( $n = 1, 2, \dots, N$ ) are unknown complex coefficients.

As suggested by (4), we have chosen the expansion modes identical to the test modes. This is termed a Galerkin solution [5]. Inserting (4) into (3) yields the system of simultaneous linear equations

$$\sum_{n=1}^N I_n Z_{mn} = V_m \quad m = 1, 2, \dots, N \quad (5)$$

where

$$Z_{mn} = - \int_{S_n} \int E_m \cdot J_n ds \quad (6)$$

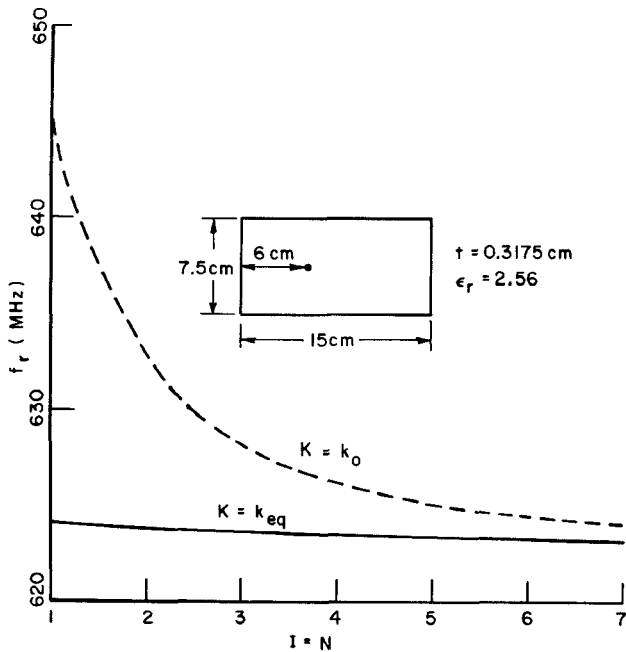
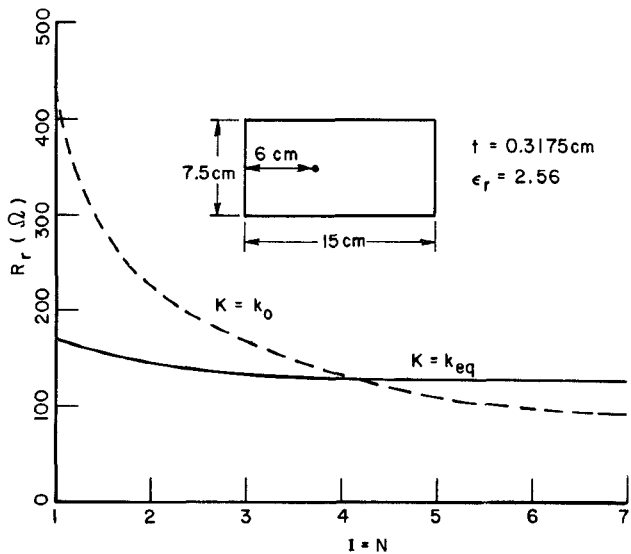
$$V_m = \int_L E_m \cdot J_i dl \quad (7)$$

and  $S_n$  is the surface of the  $n$ th expansion mode. Equations (6) and (7) are evaluated in the Appendix for parallel or skew modes.

The convergence and accuracy of the MM solution is dependent upon how well the finite sum on the right-hand side of (4) approximates the true  $J_s$ . Thus the choice of the  $J_n$  is a crucial step in the MM solution. Our previous experience with plates in free space [6] indicates that the piecewise-sinusoidal surface-patch dipole is a reasonable choice. Referring to Fig. 6, for a dipole of width  $w_m$  and length  $2h_m$ , which is centered on the  $z$ -axis

$$J_m = \frac{\sin K(h_m - |x|)}{w_m \sin Kh_m} \hat{x}. \quad (8)$$

In general, two orthogonal and overlapping arrays of dipole modes are placed on each patch, in exactly the same manner as is used in the surface patch solution for plates in free space [7]. For plates in free space, we have used  $K = k_0$  = free-space wavenumber. However, for microstrip antennas this is not the optimum choice, and further, the convergence of the solution is very dependent upon the choice for  $K$ . This is because the input impedance of a microstrip is dependent upon the slope or divergence of the current  $J_s$  at the feed point. The dependence of the convergence upon the choice of  $K$  is illustrated in Figs. 2 and 3. Here, we plot the computed resonant frequency and resonant

Fig. 2. Convergence of resonance frequency for two values of  $K$  ( $N$  odd).Fig. 3 Convergence of resonance resistance for two values of  $K$  ( $N$  odd).

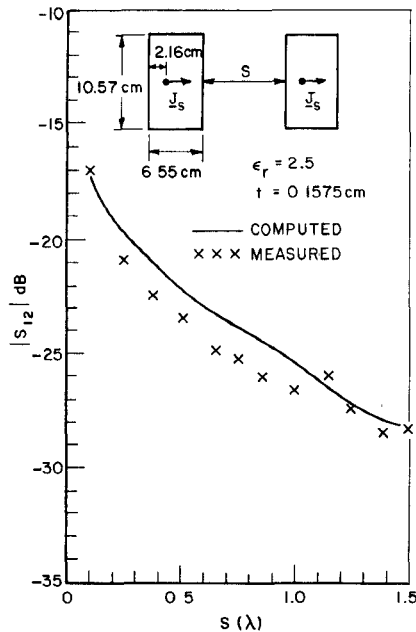
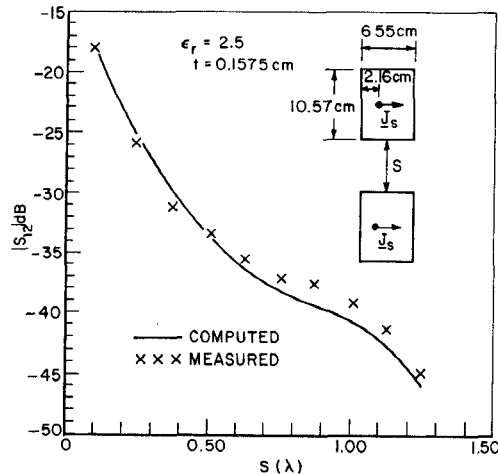
resistance versus the number ( $I = N$  odd) of expansion modes on a single microstrip patch. Note only the  $\hat{x}$ -polarized modes are used. The resonant frequency is that frequency where the input impedance is purely resistive. The resonant resistance is the input resistance at the resonant frequency. Curves are shown for  $K = k_0$  and for  $K = k_{eq} = \omega\sqrt{\mu_0\epsilon_{eq}}$ , where [8]

$$\epsilon_{eq}/\epsilon_0 = \frac{\epsilon_r + 1}{2} + \frac{\epsilon_r - 1}{2} \left[ 1 + \frac{10t}{W} \right]^{-1/2}. \quad (9)$$

Note the rapid convergence with  $k_{eq}$  versus that with  $k_0$ . In all data to follow,  $K = k_{eq}$ .

### III. COUPLED MICROSTRIPS

A significant advantage of the moment-method solution is that coupled microstrips can be treated with no additional theory than that for the isolated microstrip. Figs. 4 and 5 show computed  $E$

Fig. 4.  $E$ -plane coupling for identical microstrips.Fig. 5.  $H$ -plane coupling for identical microstrips.

and  $H$  plane coupling, for identical microstrips, versus separation, compared with measurements by Jedlicka *et al.* [9]. The magnitude of the scattering parameter  $S_{12}$  is shown to conform with the measurements. For the data, the isolated microstrips were resonant with a  $50\Omega$  resistance. This occurred at 1417 MHz for the computations, and at 1410 MHz for the measurements. There is generally good agreement between computed and measured results. Figs. 4 and 5 were calculated with  $I = J = 1$   $\hat{x}$ -polarized mode per patch and required about 60 s per data point on a VAX 11/780 (about 3 times slower than an IBM 370).

### IV. CONCLUSIONS

We have demonstrated the accurate and efficient computation of the mutual impedance between rectangular microstrip antennas. Also, exact expressions for the mutual impedance between skew modes on a grounded dielectric slab were given. This type of information is useful in the design of microstrip arrays, especially if low sidelobes are desired.

## APPENDIX

### MUTUAL IMPEDANCE

In this appendix, we will present the exact expressions for the mutual impedance between two surface-patch dipole modes on a lossy grounded dielectric slab. The mutual impedance between a surface-patch mode and the current  $\mathbf{J}_t$ , required in (7) will also be presented. Fig. 6 shows two surface-patch dipole modes, of current densities  $\mathbf{J}_m$  and  $\mathbf{J}_n$ , located on the surface of a grounded dielectric slab of real permeability  $\mu_2$  and complex permittivity  $\epsilon_2$ . The ambient medium is free space with parameters  $\mu_1$  and  $\epsilon_1$ . The  $e^{j\omega t}$  time dependence is suppressed. Mode  $m$  is centered with respect to the  $z$ -axis and is polarized in the  $\hat{x}$ -direction. Mode  $n$  is staggered a distance  $x_0$  in the  $x$ -direction and a distance  $y_0$  in the  $y$ -direction. Mode  $\mathbf{J}_n$  is at an angle  $\alpha$  with respect to the  $x$ -axis.

The mutual impedance between modes  $m$  and  $n$  is given by

$$Z_{mn} = - \int_n \mathbf{E}_m \cdot \mathbf{J}_n ds \quad (A1)$$

where the integration is over the surface of mode  $n$ . The first step in finding  $Z_{mn}$  will be to find  $\mathbf{E}_m$  at  $z = t$ , i.e., at the surface of the slab.

Mode  $m$  will be a separable function of  $x$  and  $y$ , i.e.,

$$\mathbf{J}_m(x, y) = \hat{x}J_m(x, y) = \hat{x}X_m(x)Y_m(y) \quad (A2)$$

where  $X_m(x)$  and  $Y_m(y)$  are even functions of  $x$  and  $y$ , respectively. The transform of  $X_m(x)$ , denoted  $\bar{X}_m(\beta)$ , is

$$\bar{X}_m(\beta) = 2 \int_0^\infty X_m(x) \cos \beta x dx. \quad (A3)$$

Similarly

$$\bar{Y}_m(f) = 2 \int_0^\infty Y_m(y) \cos fy dy. \quad (A4)$$

The fields in regions 1 and 2 are expressed in terms of TE and TM to  $z$ -modes. The field components are expressed in integral forms in terms of eigenfunctions and spectral distribution functions. The spectral functions are determined by matching the boundary conditions at  $z = t$ . The result is that the exact tangential electric field at  $z = t$  is given by

$$E_{xm} = \int_0^\infty \int_0^{\pi/2} F_x \cos \beta x \cos fy d\phi dk \quad (A5a)$$

$$E_{ym} = \int_0^\infty \int_0^{\pi/2} F_y \sin \beta x \sin fy d\phi dk \quad (A5b)$$

where

$$F_x = \frac{-\sinh gt}{j\omega\epsilon_2\pi^2k} \left[ \frac{f^2\gamma_2^2}{\mu_r\gamma \sinh gt + g \cosh gt} + \frac{\epsilon_{rc}g\beta^2\gamma}{\epsilon_{rc}\gamma \cosh gt + g \sinh gt} \right] \cdot \bar{X}_m(\beta) \bar{Y}_m(f) \quad (A6a)$$

$$F_y = \frac{-\sinh gt}{j\omega\epsilon_2\pi^2k} \left[ \frac{\gamma_2^2}{\mu_r\gamma \sinh gt + g \cosh gt} + \frac{\epsilon_{rc}\gamma g}{\epsilon_{rc}\gamma \cosh gt + g \sinh gt} \right] \cdot \beta f \bar{X}_m(\beta) \bar{Y}_m(f) \quad (A6b)$$

and where  $\epsilon_{rc} = \epsilon_2/\epsilon_1$ ,  $\mu_r = \mu_2/\mu_1$ ,  $\gamma_2 = j\omega\sqrt{\mu_2\epsilon_2}$ ,  $k^2 = \beta^2 + f^2$ ,  $\beta = k \cos \phi$ ,  $f = k \sin \phi$ ,  $g^2 = k^2 + \gamma_2^2$ , and  $\gamma^2 = k^2 - \omega^2\mu_1\epsilon_1$ .  $Z_{mn}$  can now be found by inserting (A5) and (A6) into (A1) and performing the surface integral over mode  $n$  in closed form.

Referring to Fig. A1, mode  $\mathbf{J}_n$  is written as a separable function of  $x'$  and  $y'$

$$\mathbf{J}_n(x', y') = \hat{x}J_n(x', y') = \hat{x}X_n(x')Y_n(y'). \quad (A7)$$

Mode  $\mathbf{J}_n$  makes an angle  $\alpha$  with respect to the  $x$ -axis and is

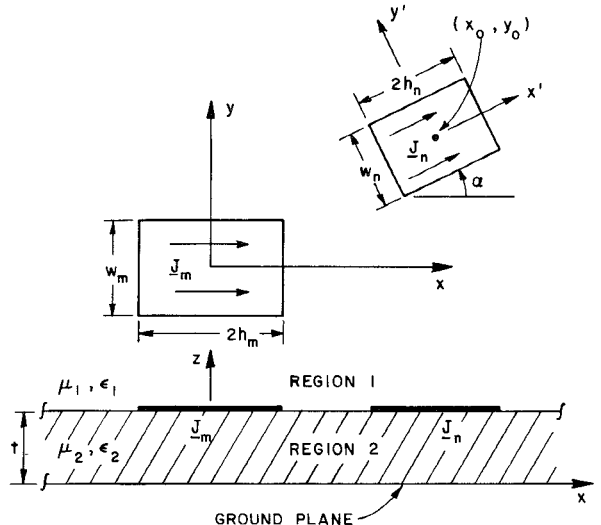


Fig. 6. Two surface-patch dipole modes on a grounded dielectric slab.

centered at  $(x, y) = (x_0, y_0)$ . Equation (A1) becomes

$$Z_{mn} = - \int_{-w_n/2}^{w_n/2} \int_{-h_n}^{h_n} \mathbf{E}_m \cdot \mathbf{J}_n dx' dy' = - \int_{-\infty}^{\infty} \int_{-\infty}^{\infty} \mathbf{E}_m \cdot \mathbf{J}_n dx' dy' \quad (A8)$$

where the limits on the integral can be removed to infinity since  $\mathbf{J}_n$  is zero exterior to mode  $n$ . Inserting (A5) into (A8) yields

$$Z_{mn} = - \int_0^\infty \int_0^{\pi/2} \left\{ \frac{F_x}{4} \sum_i \sum_l e^{j(i\beta x_0 + lf y_0)} \bar{X}_n(\beta') \bar{Y}_n(f') \cos \alpha + \frac{F_y}{4} \sum_i \sum_l i l e^{j(i\beta x_0 + lf y_0)} \bar{X}_n(\beta') \bar{Y}_n(f') \sin \alpha \right\} d\phi dk \quad (A9)$$

where

$$\beta' = i\beta \cos \alpha + lf \sin \alpha = k(i \cos \phi \cos \alpha + l \sin \phi \sin \alpha) \quad (A10a)$$

$$f' = lf \cos \alpha - i\beta \sin \alpha = k(l \sin \phi \cos \alpha - i \cos \phi \sin \alpha). \quad (A10b)$$

In deriving (A9) we used the identities

$$\cos \beta x \cos fy = \frac{1}{4} \sum_i \sum_l e^{j(i\beta x + lf y)} \quad (A11a)$$

$$\sin \beta x \sin fy = \frac{1}{4} \sum_i \sum_l i l e^{j(i\beta x + lf y)} \quad (A11b)$$

where  $\sum_l$  means  $\sum_{l=1}^1$  excluding  $l = 0$ .

For the special case of parallel modes,  $\alpha = 0$ , and (A9) reduces to

$$Z_{mn} = - \int_0^\infty \int_0^{\pi/2} F_x \bar{X}_n(\beta) \bar{Y}_n(f) \cos \beta x_0 \cos fy_0 d\phi dk. \quad (A12)$$

If all transforms can be obtained in closed form, then (A9) expresses the mutual impedance with two numerical integrations required.

Here we make the following choice for the modes (see (A2) and (A7)):

$$X_m(x) = \sin K(h_m - |x|) / \sin Kh_m \quad (A13)$$

$$Y_m(y) = 1/w_m \quad (A14)$$

and similarly for mode  $n$ . In this case, the transforms are

$$\bar{X}_m(\beta) = \frac{2K(\cos \beta h_m - \cos Kh_m)}{\sin Kh_m(K^2 - \beta^2)} \quad (A15)$$

$$\bar{Y}_m(f) = \frac{\sin(fw_m/2)}{(fw_m/2)}. \quad (A16)$$

Note that when (A15) and (A16) are substituted into (A12), the only place that the stagger between the modes enters is the factor  $\cos \beta x_0 \cos fy_0$ .

It should be noted that in evaluating (A9) or (A12) for real  $\epsilon_{rc}$  (i.e., lossless slab), the integrand is singular when  $k$  satisfies

$$g \sinh gt + \epsilon_{rc} \gamma \cosh gt = 0. \quad (A17)$$

If  $\epsilon_{rc}$  is complex (i.e., a lossy slab), then the values of  $k$  which satisfy (A17) are complex, and the integrand will be large but not singular. In either case, numerical integration in the vicinity of the singularity or near singularity will be difficult and time consuming. One should perform this region of the integral analytically using residue theory or similar techniques.

The right-hand vector in the moment-method solution is given by (6). Omitting all details, for a surface-patch mode center at the origin (i.e., mode  $J_m$  in Fig. 6) and  $J_i$  located at  $(x_f, y_f)$  the result is

$$V_m = \frac{j}{\pi \omega \epsilon_1} \int_0^\infty Q \int_0^{\pi/2} \beta \bar{X}_m \bar{Y}_m \sin \beta x_f \cos fy_f d\phi dk \quad (A18)$$

where

$$Q = \frac{k \gamma \sinh gt}{g(g \sinh gt + \epsilon_{rc} \gamma \cosh gt)}. \quad (A19)$$

## REFERENCES

- [1] *IEEE Trans. Antennas Propagat.*, vol. AP-29, Jan. 1981.
- [2] N. G. Alexopoulos and I. E. Rana, "Mutual impedance computation between printed dipoles," *IEEE Trans. Antennas Propagat.*, vol. AP-29, pp. 106-111, Jan. 1981.
- [3] E. H. Newman and P. Tulyathan, "Analysis of microstrip antennas using moment methods," *IEEE Trans. Antennas Propagat.*, vol. AP-29, pp. 47-53, Jan. 1981.
- [4] V. H. Rumsey, "Reaction concept in electromagnetic theory," *Phys. Rev.*, vol. 94, no. 6, pp. 1483-91, June 1954.
- [5] R. F. Harrington, *Field Computations by Moment Methods*. New York: MacMillan, 1968.
- [6] E. H. Newman and D. M. Pozar, "Electromagnetic modelling of composite wire and surface geometries," *IEEE Trans. Antennas Propagat.*, vol. AP-26, pp. 784-88, Nov. 1978.
- [7] —, "Considerations for efficient wire/surface modeling," *IEEE Trans. Antennas Propagat.*, vol. AP-28, pp. 121-124, Jan. 1980.
- [8] P. Silvester, "TEM wave properties of microstrip transmission lines," *Proc. IRE*, vol. 115, pp. 43-48, Jan. 1968.
- [9] R. P. Jedlicka, M. T. Poe, and K. R. Carver, "Measured mutual coupling between microstrip antennas," *IEEE Trans. Antennas Propagat.*, vol. AP-29, pp. 147-149, Jan. 1981.

## Analysis of the Hybrid Modes for an Eccentrically Cladded Fiber

ANDREAS D. LYRAS, JOHN A. ROUMELIOTIS,  
JOHN D. KANELLOPOULOS, AND JOHN G. FIKIORIS

**Abstract**—This paper examines the hybrid-cladding modes of an eccentrically cladded three-layer dielectric fiber. The solutions are specialized to small eccentricities, and exact closed-form expressions for the normal-

Manuscript received June 25, 1982; revised July 5, 1983.

The authors are with the Department of Electrical Engineering, National Technical University of Athens, Athens 147, Greece.

ized deviations of the cutoff wavenumbers from those of the concentric case are determined. Numerical results for various types of hybrid-cladding modes of the fiber are given. For certain values of the parameters, it is possible to enhance the operating bandwidth of the basic hybrid mode  $HE_{11}$  over the conventional concentric fiber because its cutoff frequency can be shown to remain zero.

## I. INTRODUCTION

This paper extends the results of a previous work [1] for the symmetrical modes in a cladded fiber to the more interesting and practical case of its hybrid modes. The eccentricity  $d$  (Fig. 1) might arise either as a manufacturing defect or as an intentional feature of the fiber with the purpose of improving the operating characteristics. The main difference in the analysis of the two cases lies in the complexity of the limiting forms for the cutoff condition of the various hybrid modes. The same final expression for the cutoff wavenumbers of the cladding modes  $k_{nm}(d)$  is obtained

$$k_{nm}(d) = k_{nm}(0) [1 + g_{nm}(k_{nm}(0)d)^2] \quad (1)$$

where for the normalized deviations  $g_{nm}$ , closed-form but more complicated expressions are developed. For certain values of the parameters, it is possible in conjunction with the results of [1] to enhance the operating bandwidth of the basic hybrid mode  $HE_{11}$  over the conventional concentric fiber. Numerical results for various hybrid modes and for several profiles of cladded fibers are also included.

## II. THE ANALYSIS

Referring to the waveguide of Fig. 1, which is a perturbation of the more commonly known concentric structure and with assumed harmonic time dependence  $\exp(i\omega t)$ , the longitudinal field components  $E_{z_i}^j(P)$  and  $H_{z_i}^j(P)$  can be expanded in terms of the appropriate Bessel and azimuthal functions as follows:

$$E_{z_1}^1(P) = \sum_{n=0}^{\infty} \left[ \frac{\alpha_n}{\alpha'_n} \cos(n\theta_1) + \frac{\beta_n}{\beta'_n} \sin(n\theta_1) \right] J_n(k_1 r_1) e^{-i\gamma z} \quad (2)$$

$$H_{z_1}^1(P) = \sum_{n=0}^{\infty} \left\{ \left[ \frac{A_n}{A'_n} J_n(k_2 r_1) + \frac{B_n}{B'_n} B_n' Y_n(k_2 r_1) \right] \cos(n\theta_1) + \left[ \frac{C_n}{C'_n} J_n(k_2 r_1) + \frac{D_n}{D'_n} D_n' Y_n(k_2 r_1) \right] \sin(n\theta_1) \right\} e^{-i\gamma z} \quad (3)$$

$$E_{z_2}^2(P) = \sum_{n=0}^{\infty} \left[ \frac{A_{3n}}{A'_{3n}} \cos(n\theta_2) + \frac{B_{3n}}{B'_{3n}} \sin(n\theta_2) \right] H_n^{(1)}(k_3 r_2) e^{-i\gamma z} \quad (4)$$

where  $k_i = (\omega^2 \mu_i \epsilon_i - \gamma^2)^{1/2}$ ,  $i = 1, 2, 3$ . The superscript 1 or 2 denotes the reference center of coordinates (see Fig. 1). The subscript 1, 2, or 3 denotes the region of space.

The boundary conditions at  $r_1 = R_1$  and  $r_2 = R_2$  require that the tangential components of  $\bar{E}$ ,  $\bar{H}$  be continuous [1]. This further necessitates the re-expansion of the field components  $E_{z_2}^1, H_{z_2}^1$  in terms of cylindrical circular wavefunctions around the axis  $0_2$  using translational addition theorems [2].

The end result is (4) and (5) of [1]. We then turn our attention to the hybrid modes of the fiber by considering values of  $p \geq 1$ , whereas the symmetrical modes of [1] correspond to  $p = 0$ .